Beam manipulation of transmission co-polarization wave based on multilayer encoding metamaterials

FUHAI LIU[a], BO FANG[b,*], JING FAN[c], XUETAO CHENG[c], ZHIGANG YAN[d], HAIYONG GAN[e],
YINGWEI HE[e], HAO YU[f], CHENXIA LI[f], XUFENG JING[f,g,*], ZHI HONG[g]
[a]*Special Equipment College, Hangzhou Vocational & Technical College, Hangzhou 310018, China*
[b]*College of Metrology & Measurement Engineering, China Jiliang University, Hangzhou 310018, China*
[c]*Chang Qing Oil Field Branch Company, Technical monitoring center, Xi'an, ShanXi, China*
[d]*Hangzhou Dahua Apparatus Manutacture Co., Ltd., China*
[e]*National Institute of Metrology, Beijing, China*
[f]*Institute of Optoelectronic Technology, China Jiliang University, Hangzhou 310018, China*
[g]*Centre for THz Research, China Jiliang University, Hangzhou 310018, China*

We propose a multilayer unit cell with a mixture of metal and dielectric materials to configurate the encoding metamaterials. The higher transmittance with more than 0.9 and the phase change from $0°$ to $360°$ are critically designed for unit cells corresponding to different encoded particles. Here, the parallel encoding method and the checkerboard encoding method are adopted to construct the encoding metamaterials by using corresponding encoded particles. The scattering energy for co-polarization transmitted electromagnetic wave can be flexibly manipulated by using the designed encoding metamaterials. The far field scattering of transmitted wave is numerically simulated by using finite integral method. According to the generalized Snell's law, it is found that the calculated theoretical deflection angles agree well with that of numerical simulation.

1. Introduction

Electromagnetic metamaterials have received extensive attention due to their unique electromagnetic properties, and have become the frontier interdisciplinary subject in the fields of physics, chemistry, materials and information [1-20]. The study of metamaterials mainly focused on periodic or aperiodic structures of sub-wavelength dimensions, which can be characterized by uniform macroscopic media parameters. By designing a specific metamaterial, free control of equivalent parameters can be realized, thereby achieving the function of freely regulating electromagnetic waves and obtaining abnormal physical characteristics and phenomena [21-25]. For example, current metamaterials can be used in areas, such as negative refraction, perfect lenses, zero-refractive materials, tunneling effects, stealth cloaks, and transformation optics [26-32]. However, research and analysis of metamaterials typically employ macroscopically continuous, uniform or non-uniform equivalent structural parameters, to manipulation of electromagnetic wave.

Recently, Giovampaola and Engheta *et al.* proposed a method for constructing "metamaterial bytes" by spatially mixing "digital metamaterial bits" [33]. At the same time, Cui et al. proposed the concepts of "encoding metamaterials", "digital metamaterials" and "programmable metamaterials" [34]. Programmable metamaterials mean that metamaterials can achieve different functions through digital control, thus realizing digital regulation and real-time regulation of electromagnetic waves. In the past few years, the encoding metamaterials have experienced rapid development. Specially, Zhang *et al.* proposed a digital metasurface platform that can be programmed optically to implement electromagnetic functions [35]. Also,

Zhang *et al.* proposed a polarization-controlled dual-programmable metasurface with modular control circuits, which enabled a dibit encoding capability in modifying the phase profiles [36].

Different metal patterns, different applicable working bands, and different materials for the encoding metamaterials are constantly proposed and designed [37-41]. However, due to the simplicity of phase control of metamaterials in reflective mode, most of the current research on coded metamaterials focuses on the reflection mode. It is known that the encoding metamaterials in the transmission mode are developed slowly. Recently, in order to solve the problem of single function of the encoding metamaterials, Liu *et al.* proposed a transmissive-reflective dual-function coded metamaterial [42]. However, these coded metamaterials in transmission mode mainly focused on the manipulation of electromagnetic wave with cross polarization.

Based on the application of co-polarization transmission mode encoding metamaterials, we propose a multi-layer encoding metamaterial in microwave frequency. By using finite integral method, the transmission coefficient and phase change of encoding unit structure can be numerically calculated and optimized. The phase control of $0^{\circ}\sim360^{\circ}$ with co-polarization of transmission electromagnetic wave can be obtained. These unit cells of encoding particles can be reasonably encoded to construct encoding metamaterial to manipulate beam of transmissive wave.

2. Generalized Snell's law for coding metamaterials

Generally, when a beam of light is incident on an interface from one medium to another, the reflection or refraction occurs. The incident, reflected, and refracted rays are in the same plane. As shown in Fig. 1(a), the refractive indices of the media on both sides of the interface are n_1 and n_2, respectively. The angle between the incident ray and the normal direction is θ_i, and the angle between the refracted ray and the normal direction is θ_t. The incident ray and the refracted ray

satisfy the following relationship as

$$n_1 sin\theta_i = n_2 sin\theta_t \qquad (1)$$

However, when the interface between the two media is a super interface, abnormal refraction or reflection phenomenon different from conventional optics will occur. This is due to the abrupt phase change when the light passes through the metasurface. Therefore, the traditional Snell's law will no longer be applicable on this super interface. According to Fermat's theorem and Maxwell's equations, the applicable generalized law of reflection and refraction can be derived.
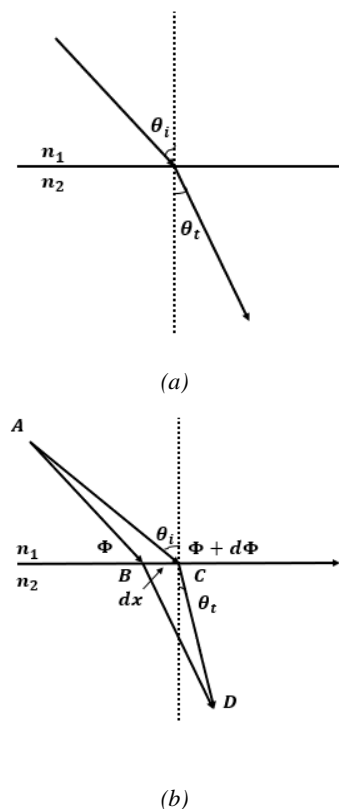

(a)

(b)

Fig. 1. (a)Schematic diagram for general transmissive beam at interface, (b) Refraction with phase difference on the interface

According to the Fermat principle, the total phase of the light wave in the actual optical path should take the extreme value. A phase sudden change of $\Phi(r_s)$ is introduced on the interface, and $\Phi(r_s)$ is a function of r_s, where r_s is the coordinate on the interface. As shown

in Fig. 1(b), when a beam of light is incident on the interface between the media at an angle θ_i, the angle of refraction is θ_t. Assuming that there are two paths from point A to point D as ABD and ACD, the phase difference between them is zero when they are infinitely close to the actual optical path. Then, we can obtain

$$(k_0 n_1 sin\theta_i dx + \Phi + d\Phi) - (k_0 n_2 sin\theta_t dx + \Phi) = 0$$
$$(2)$$

where dx represents the distance between two points on the x-axis of the interface, Φ and $\Phi+d\Phi$ represent respectively the phase change of the interface at two points. n_1 and n_2 represent the refractive index of the medium on both sides of the interface. k_0 represents the wave number in vacuum. In Eq.(2), the propagation path of light can be determined by the refractive index on both sides of the interface and the angle of incidence of the light. According to Eq.(2) with the phase change along the interface to be constant, it is obtained for transmissive modal of incident wave as

$$n_2 sin\theta_t - n_1 sin\theta_i = \frac{\lambda_0}{2\pi}\frac{d\Phi}{dx}$$
$$(3)$$

where λ_0 represents the wavelength in vacuum, and Eq.(3) shows the generalized law of refraction. If the refraction angle θ_t in Eq.(2) is replaced by the reflection angle θ_r, the generalized law of reflection can be similarly derived as

$$n_1 sin\theta_r - n_1 sin\theta_i = \frac{\lambda_0}{2\pi}\frac{d\Phi}{dx}$$
$$(4)$$

3. Unit cell of encoding metamaterials

Firstly, in order to construct an encoding metamaterials with co-polarization transmission, the unit cells of metamaterials should be designed. Here, we propose a unit cell with multilayer microstructure to realize co-polarization transmission with the phase change from $0°$ to $360°$. As shown in Fig. 2, the unit structure is composed of five copper layers (C1, C2, C3, C4, C5) and four dielectric layers (M). In order to clearly demonstrate the configuration of unit cell, the schematic

diagram of unit cell in Fig.2 is enlarged between layers. In our design and calculation, the multilayer structure is appressed. The thickness of the five copper layers is 0.018 mm. For the layers of C1, C2, C4 and C5, the length in x direction is zx, the overhang length in x direction is x, and the length of metal is zy in y direction. The copper layer C2 is the same as C4, and has a length p1 in the y direction. The lengths of the copper layers C1 and C5 in the y direction are y1 and y2, respectively. The copper layer C3 has a slotted square with a side length of p. The slot shows the length of l and the width of w. The four dielectric plates (M) with the dielectric constant ($\varepsilon_r=$ 2.65) are identical with the side length of p and the thickness of h.
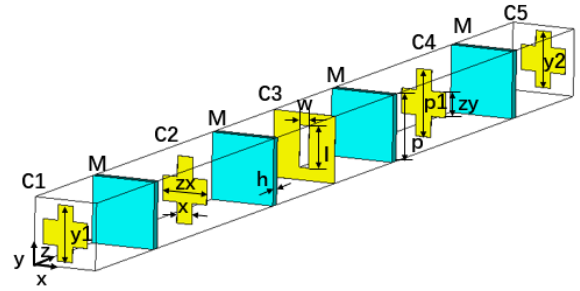

Fig. 2. Schematic diagram of unit cell for encoding metamaterials (color online)

In Fig. 2 for unit cell of encoding metamaterials, it can be found that the unit structure shows asymmetry characteristic, so that it can control different polarization mode of incident light. When the incident light is incident on unit cell under x-polarization, the value of zx can be changed to change the transmittance and the transmission phase; When the incident light is incident under the y-polarization, the values of y1 and y2 can be changed to change the transmittance and the transmission phase. However, the above unit structure has a total of nine layers. In order to avoid too much light attenuation when incident light is incident through the unit structure, the copper layer C3 is designed as a slotted structure, providing an aperture coupling for efficient passage of incident light.

In the process of unit cell optimization, it is necessary to change the length zx of the metal piece when the x-polarized wave is incident. As shown in Fig. 2, the

length of zx needs to be smaller than the side length p of the medium, but the length of zx needs to be larger than the edge length x of the metal piece. At the targeted frequency band, the effective length is determined using a dichotomy between intervals [x, p]. Similarly, the transmission characteristics can be controlled by the length of y1 and y2 when a y-polarized electromagnetic wave is incident. After optimization, the "0" code represents $0°$ of transmission phase and the "1" code represents $180°$ of transmission phase when the incident wave is x- or y-polarized at 15GHz. The corresponding geometric parameters for unit cells of "0" code and "1" code are demonstrated in Table 1.

Table 1. Geometric parameters for unit cells of code "0" and code "1"

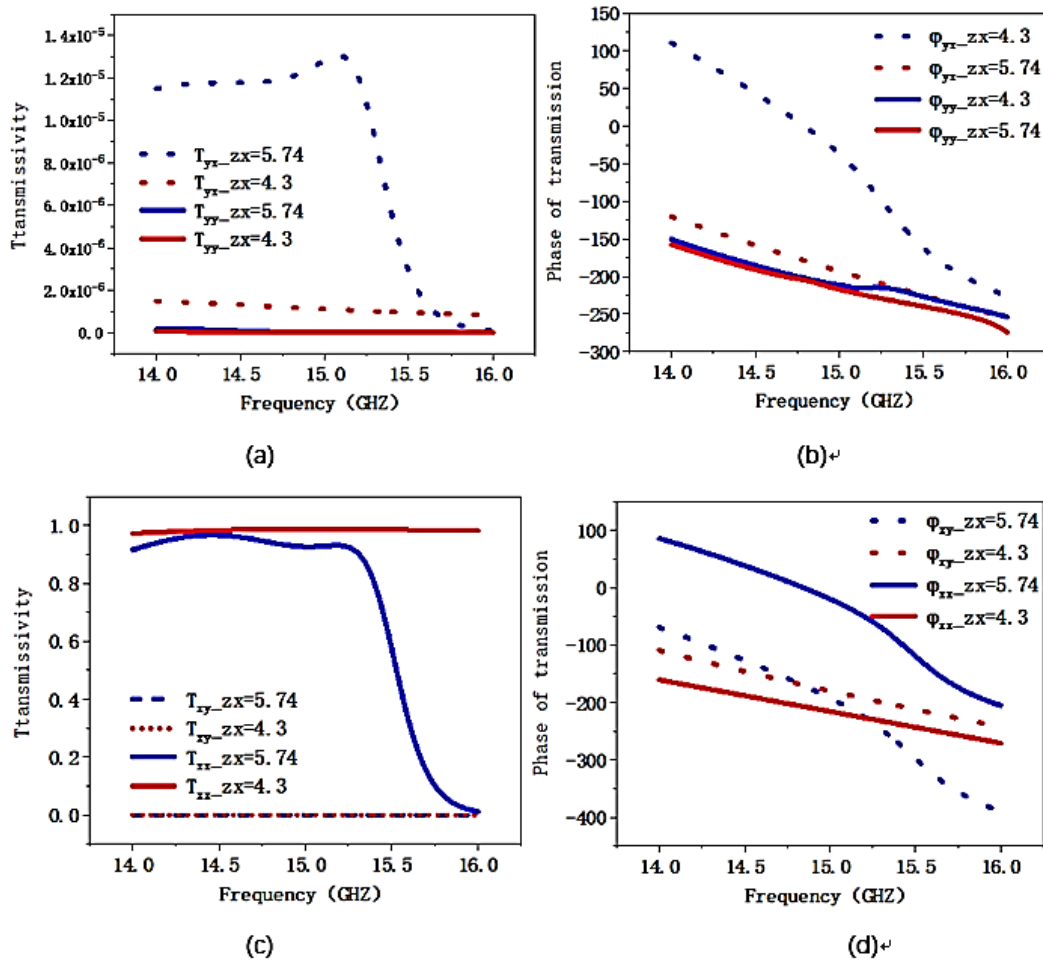| parameters（mm）	"0"	"1"
p	8	8
$p1$	8	8
zx	4.3	5.74
zy	3	3
x	2	2
$y1$	6.7	6.7
$y2$	6.7	6.7
h	1	1
w	1.2	1.2
l	5	5

(a)

(b)

(c)

(d)

Fig. 3. (a) Transmittance (co-polarization and cross polarization) and (b) phase change (co-polarization and cross polarization) for the unit cells of code "0" and code "1" with different geometric parameters when the y-polarized wave is incident; (c) Transmittance (co-polarization and cross polarization) and (d) phase change (co-polarization and cross polarization) for the unit cells of code "0" and code "1" with different geometric parameters when the x-polarized wave is incident (color online)

According to the geometric parameters in Table 1, the transmission and phase change are calculated for the periodic structure of the unit cells when the *x*- or *y*-polarized wave is incident. Fig. 3 shows the transmittance and phase change of the co-polarization and cross polarization. It can be seen in Fig. 3(a) that the transmittance for both co-polarization and cross polarization is almost zero when a y-polarized wave is incident. The corresponding phase change of transmitted wave is demonstrated in Fig. 3(b). When the *x*-polarized wave is incident, the transmittance higher more than 0.9 for the co-polarization is revealed from 14GHz to 15.3GHz when the geometric parameter of *zx* is 5.74 mm or 4.3 mm. In Fig. 3(d), it can be seen that the phase difference of the transmitted light between unit cells with different *zx* is almost 180° at 15GHz. The detailed value for phase difference is demonstrated in Table 2. However, for the cross polarization in Fig. 3(c), the transmittance of the transmitted light is almost zero for both unit cells. Thus, we will construct a encoding metamaterial with these two unit cells to research its co-polarization transmitted beam manipulation when the x-polarized wave is incident.

Table 2. Phase and phase difference between two unit cells

Frequency (GHZ)	φ (*zx* = 4.3mm)	φ (*zx* = 5.74mm)	Δφ
15.114	-35.9	-221.8	185.8
15.126	-37.8	-222.5	184.6
15.138	-39.7	-223.1	183.4
15.15	-41.6	-223.8	182.1
15.162	-43.6	-224.5	180.8
15.17	-44.9	-224.8	179.9
15.174	-45.6	-225.1	179.5
15.186	-47.6	-225.8	178.1
15.198	-49.7	-226.4	176.7
15.21	-51.9	-227.1	175.2

4. Multilayer transmission type coding metamaterials

According to the design of unit cells with code "0" and code "1" above, we will construct encoding metamaterials by using different encoding methods to manipulate the transmitted beam. Figure 4(a) shows a parallel distributed code method in the form of "010101.../010101..." for 1 bit binary encoding. Figure 4(b) shows a checkerboard distributed code method in the form of "010101.../101010...".
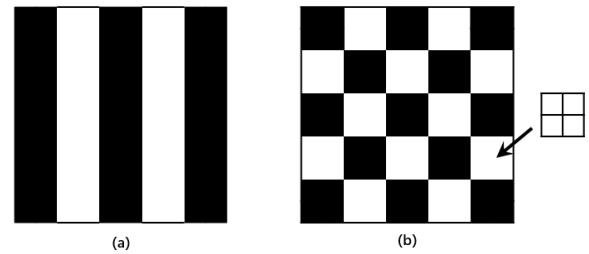

Fig. 4. 1-bit parallel distributed coding and checkerboard distributed coding

In Fig. 4, the black portion represents code "0" in the binary code, and the white portion represents code "1" in the binary code. In order to more accurately control the beam of transmitted wave, a large number of digital elements should be constructed in encoding metamaterials. Each element of encoding metamaterial consists of "2 x 2" unit cells with code "0" or code "1". A whole encoding metamaterial consist of "5 x 5" elements. After the unit structure design is completed, the cell structure with *zx* equal to 4.3 mm is selected as code "0" in the binary code, and the cell structure with *zx* equal to 5.74 mm is taken as "1" in the binary code. We fix the incident frequency at 15.17GHz. The phase difference of the transmitted light corresponding to the two code particles is 179.9°.

4.1. Parallel encoding metamaterials

According to the parallel encoding method in Fig. 4(a), we construct a whole encoding metamaterial consisting of "5 x 5" elements. Each element of encoding metamaterial consists of "2 x 2" unit cells with code "0"

and code "1". When the *x*-polarized wave at 15.17 GHz is normally incident on the encoding metamaterial, the three-dimensional far field distribution of co-polarization transmitted wave is demonstrated in Fig. 5.
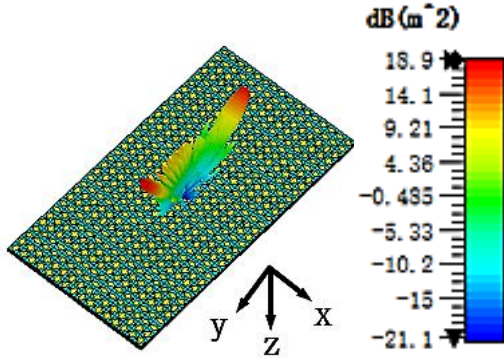

Fig. 5. 1bit parallel distributed coding 3D far field distribution (color online)

The transmitted beam is mainly divided into two beams surrounded by many side lobes, and the scattering direction is mainly concentrated in the *x* direction. According to Eq. (3), the angle of refraction can be calculated by using the generalized Snell's law as

$$\theta = sin^{-1} \lambda/_\Gamma \ , \tag{5}$$

where λ represents the wavelength of the incident light, and Γ represents the coding period. On basis of the incident frequency of 15.17 GHz and the encoding period of 32 mm, the refractive angle can be calculated as $38.17°$, which is consistent with the numerical simulation of $141.83°$ in Fig.5. We built a spherical coordinate system for three far field distribution of transmitted beam as shown in Fig.6. The direction of the refracted ray and radiant energy can be accurately defined. In Fig.6, $\overrightarrow{OM}$ denotes the refracted ray with the radiation distance of 1m. The angle between $\overrightarrow{OM}$ and the positive direction of the *z*-axis is θ, the angle between $\overrightarrow{OM}$ and the positive direction of the *x*-axis is φ. In Fig.5, the refracted beam is almost in the *yoz* plane, and it is defined as $\varphi = 90°$. Figure 7 shows the scattering energy distribution at the *yoz* plane at the radiant distance of 1m for 1-bit parallel encoding metamaterial, corresponding to that of Fig.5.

Moreover, the different encoding sequences can be constructed to obtain different scattering angles for this 1-bit encoding model. Figure 8 shows 3D scattering patterns with different scattering angles for the encoding sequences S(000111000111…) and S(0000111100001111…).
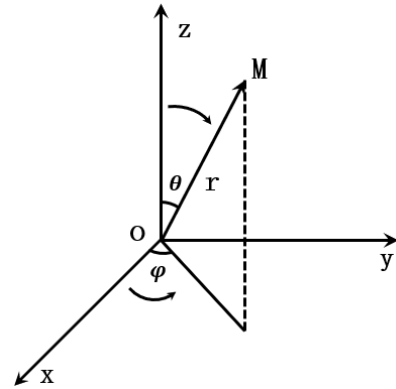

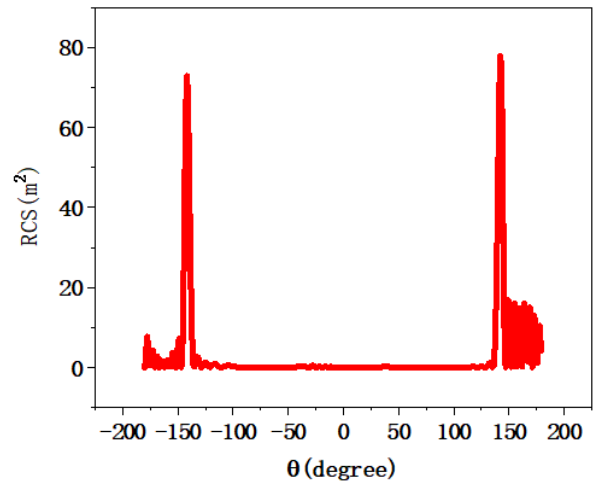*Fig. 6. Spherical coordinate system*

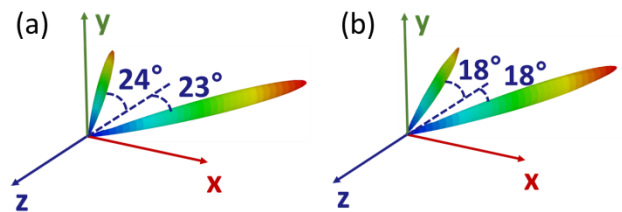*Fig. 7. Scattering energy distribution for 1bit parallel encoding metamaterial (color online)*

Fig. 8. 3D scattering patterns with different scattering angles for the encoding sequences (a) S(000111000111…) and (b) S(0000111100001111…) (color online)
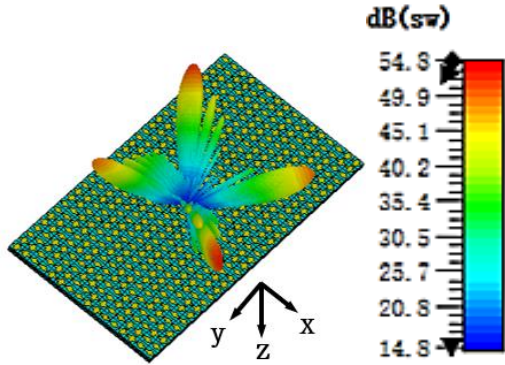
4.2. Checkerboard encoding metamaterials

Fig. 9. 3D far field distribution of scattering energy for 1bit checkerboard encoding metamaterial (color online)
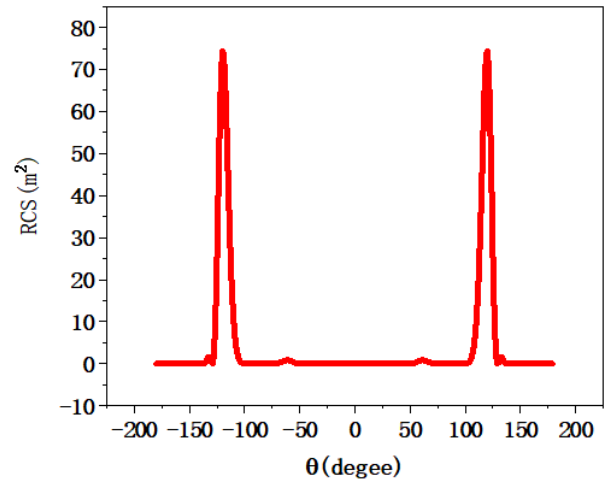

Fig. 10. Scattering energy distribution for 1bit checkerboard encoding metamaterial at φ=45° (color online)

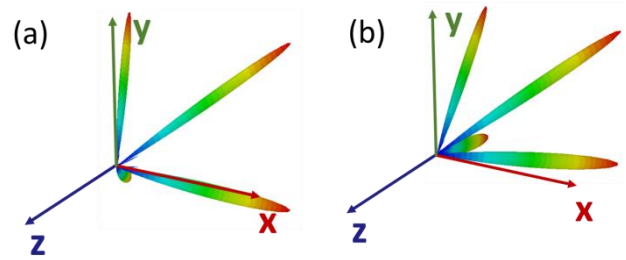*Fig. 11. 3D far field distribution of scattering energy for checkerboard encoding metamaterials. (a) S(000111…/111000…), (b) S(00001111…/11110000…) (color online)*

According to the checkerboard encoding method as shown in Fig.4(b), we construct a encoding metamaterial. A whole encoding metamaterial consists of "5 x 5" elements. Each element of encoding metamaterial consists of "2 x 2" unit cells with code "0" or code "1". The far field distribution of scattering energy is shown in Fig.9. The transmitted beam is mainly divided into four symmetrical beams, and there are a few side lobes between the four beams. Compared to the parallel encoding distribution, the scattering energy of the refracted beams formed by the checkerboard encoding metamaterial is more uniform. According to the spherical coordinate system as shown in Fig. 6, two-dimensional scattering energy distribution is shown in Fig.10 at φ=45°. Also, the theoretical calculation of scattering angle according to Eq.(3) agrees well with that of numerical simulation. Additionally, the different encoding sequences for the checkerboard encoding can be constructed to obtain different scattering angles. Figure 11 shows 3D scattering patterns with different scattering angles for the encoding sequences S(000111…/111000…) and S(00001111…/11110000…).

4.2.1. Bit encoding metamaterials

In the above section, we analyzed the beam manipulation of 1bit encoding metamaterials with code "0" and code "1". Next, we will show the beam control of 2bit encoding metamaterials. For 2bit encoding method, four different unit cell of metamaterials should be designed with the transmitted phase difference of 90°. They are respectively named as codes "00", "01", "10", and "11". After optimization, the geometrical parameters of unit cells corresponding to codes "00", "01", "10", and "11" are designed as shown in Table 3 according to the unit cell in Fig. 2.

Table 3. Codes "00", "01", "10", "11" structure parameters

Parameters	"00"	"01"	"10"	"11"
p	8	8	8	8
zx	2.2	4.3	5.35	5.74
zy	3	3	3	3
x	2	2	2	2
$y1$	6.7	6.7	6.7	6.7
$y2$	6.7	6.7	6.7	6.7
h	1	1	1	1
w	1.2	1.2	1.2	1.2
l	5	5	5	5

Based on the geometrical parameters in Table 3 for different unit cells corresponding to codes "00", "01", "10", and "11", we calculated respectively the transmittance and phase change of the periodic structure of four unit cells as a function of the incident frequency as shown in Fig.12. It can be found that the transmittance for co-polarization incident wave for four different unit cells is higher than 0.9 from 14GHz to 15.3GHz. The x-polarized wave is incident on the periodic structure of unit cells. When the incident frequency is larger than 15.3GHz, the transmittance corresponding to the unit structure of code "11" is abruptly decreased. In Fig.12(b), there is a phase difference of $90°$ between four unit cells at 15.17GHz.
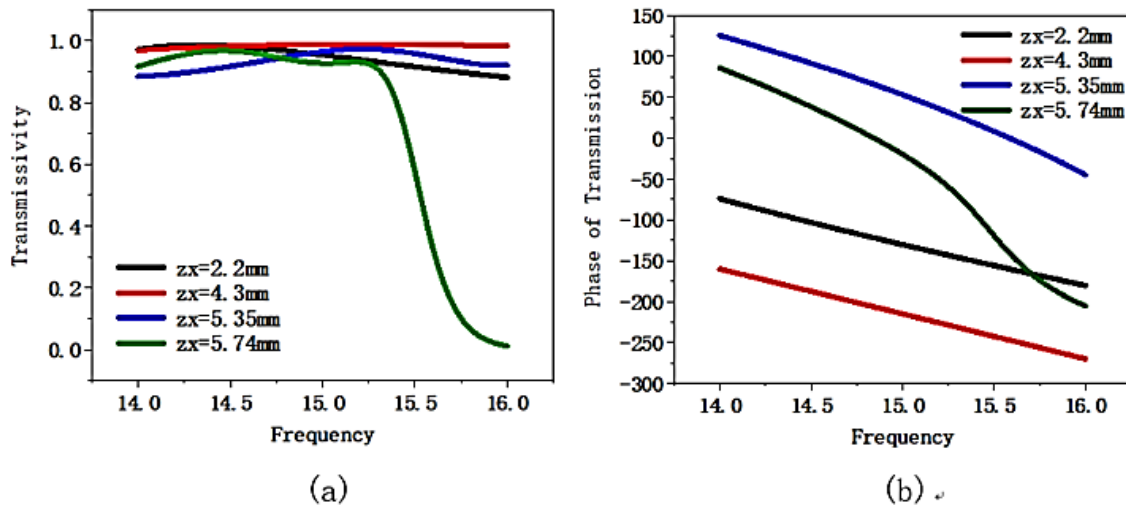

Fig. 12. (a) Transmittance and (b) phase change for co-polarization transmitted wave for four different unit cells (color online)

According to the parallel encoding method in Fig.4(a), we construct a whole encoding metamaterial consisting of "5 x 5" elements. Each element of encoding metamaterial consists of "2 x 2" unit cells with codes "00", "01", "10", and "11". When the x-polarized wave at 15.17 GHz is normally incident on the encoding metamaterial, the three-dimensional far field distribution of co-polarization transmitted wave is demonstrated in Fig. 13.
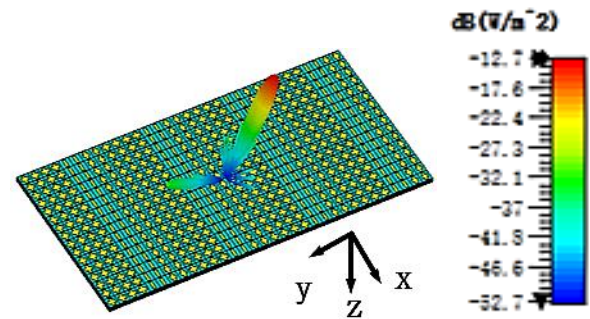

Fig. 13. 2bit parallel distributed coding 3D
far field distribution (color online)

In Fig. 13, there is only one main refracted beam of co-polarization transmitted wave for the 2bit-coded

metamaterial. However, for 1bit encoding metamaterial with parallel encoding method, there are two main scattering beams. Thus, encoding metamaterials can effectively control the number of transmitted beam and scattering angle. According to Eq.(5) with the frequency of 15.17 GHZ and the period of 64 mm respectively, we can calculated the refraction angle equal to 18.0°. According to the spherical coordinate system as shown in Fig.6, two-dimensional scattering energy distribution in the *yoz* plane is shown in Fig.14, and the deflection angle of the refraction angle is 198°. Thus, the theoretical scattering angle agrees well with that of numerical simulation. Additionally, the different encoding sequences for the 2-bit encoding can be constructed to obtain different scattering angles. Fig. 15 shows 3D scattering patterns with different scattering angles for the encoding sequences S(00011011..) and S(0000000101011101010111111…).
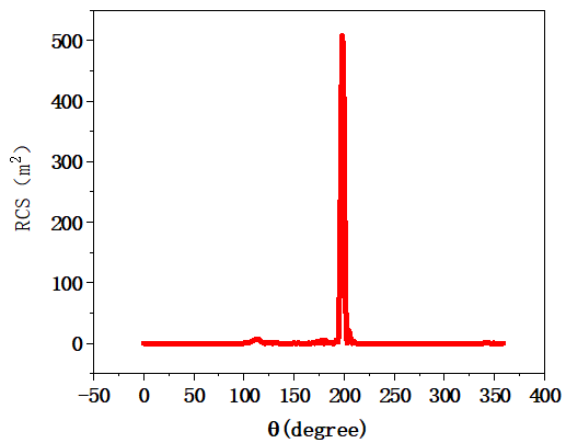

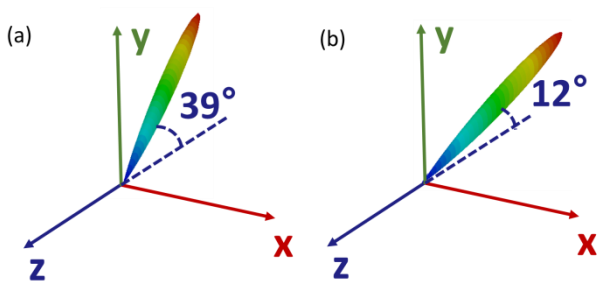*Fig. 14. Scattering energy distribution for 2bit parallel encoding metamaterial at yoz plane (color online)*

Fig. 15. 3D scattering patterns with different scattering angles for the encoding sequences (a) S(00011011..) and (b) S(0000000101011101010111111 …) (color online)

5. Conclusions

In summary, we propose a multilayer unit cell to construct encoding metamaterials. In order to realize co-polarization transmitted beam manipulation, we optimize the design of geometrical parameters of unit cells corresponding 1bit code and 2bit code. By using the finite integral method, the transmittance and the phase change of periodic structure of unit cell are detailedly calculated. According to the parallel encoding method and the checkerboard encoding method, the encoding metamaterials are constructed for 1bit encoding modal and 2bit encoding modal. Also, the far field distribution of scattering energy for the encoding metamaterials is numerically simulated.

References

[1] N. Yu, P. Genevet, M. A. Kats, F. Aieta, J. P. Tetienne, F. Capasso, Z. Gaburro, Science **334** (6054), 333 (2011).
[2] S. Teng, Q. Zhang, H. Wang, L. Liu, H. Lv, Photonics Res. **7**(3), 246 (2019).
[3] X. Luo, Z. Tan, C. Wang, J. Cao, Chin. Opt. Lett. **17**(9), 093101 (2019).
[4] W. Liang, Z. Li, Y. Wang, W. Chen, Z. Li, Photon. Res. **7**(3), 318 (2019).
[5] Y. Cui, G. Zheng, M. Chen, Y. Zhang, Y. Yang, J. Tao, T. He, Z. Li, Chin. Opt. Lett. **17**(11), 111603 (2019).
[6] T. Hou, Y. An, Q. Chang, P. Ma, J. Li, D. Zhi, L. Huang, R. Su, J. Wu, Y. Ma, P. Zhou, High Power Laser Sci. Eng. **7**(4), e59 (2019).
[7] S. Sun, Q. He, S. Xiao, Q. Xu, X. Li, L. Zhou, Nature Materials **11**(5), 426 (2012).
[8] J. Lin, J. P. Mueller, Q. Wang, G. Yuan, N. Antoniou, X. C. Yuan, F. Capasso, Science **340**(6130), 331 (2013).
[9] X. Ni, N. K. Emani, A. V. Kildishev, A. Boltasseva, V. M. Shalaev, Science **335**(6067), 427 (2012).

[10] C. Pfeiffer, N. K. Emani, A. M. Shaltout,
A. Boltasseva, V. M. Shalaev, A. Grbic, Nano
Letters **14**(5), 2491 (2014).

[11] H. X. Xu, G. M. Wang, M. Q. Qi, J. G. Liang,
J. Q. Gong, Z. M. Xu, Physical Review B **86**(20),
205104 (2012).

[12] H. Wang, J. Zheng, Y. Fu, C. Wang, X. Huang,
Z. Ye, L. Qian, Chin. Opt. Lett. **17**(5),
052303 (2019).

[13] M. Huault, D. De Luis, J. Apinaniz, M. De Marco,
C. Salgado, N. Gordillo, C. Neira,
J. A. Perez-Hernandez, R. Fedosejevs, G. Gatti,
L. Roso, L. Volpe, High Power Laser Sci. and Eng.
7(4), 60 (2019).

[14] L. Koirala, C. Park, S. Lee, D. Choi, Chin. Opt. Lett.
17(8), 082301 (2019).

[15] Shimon Rubin, Yeshaiahu Fainman, Advanced
Photonics **1**(6), 066003 (2019).

[16] A. Hanuka, K. P. Wootton, Z. Wu, K. Soong,
I. V. Makasyuk, R. J. England,
L. Schchter, High Power Laser Science and
Engineering **7**(1), e7 (2019).

[17] J. Zhao, X. Jing, W. Wang, Y. Tian, D. Zhu, G. Shi,
Opt. Laser Technol. **95**(1), 56 (2017).

[18] M. Feng, J. Wang, H. Ma, W. Mo, H. Ye, S. Qu,
Journal of Applied Physics **114**(7), 074508 (2013).

[19] H. Chen, J. Wang, H. Ma, S. Qu, Z. Xu, A. Zhang,
M. Yan, Y. Li, Journal of Applied Physics **115**(15),
154504 (2014).

[20] B. Fang, Y. Ke, L. Jiang, J. Cai, H. Gan, M. Zhang,
C. Li, Z. Hong, Appl. Phys. A **126**, 619 (2020).

[21] F. Aieta, P. Genevet, M. A. Kats, N. Yu,
R. Blanchard, Z. Gaburro, F. Capasso, Nano Letters.
12(9), 4932 (2012).

[22] Y. Deng, Z. Liu, Y. Liu, Y. Wu, Plasmonics **12**(6),
1717 (2017).

[23] L. Huang, X. Chen, B. Bai, Q. Tan, G. Jin,
T. Zentgraf, S. Zhang, Light: Science &
Applications **2**(3), e70 (2013).

[24] H. Li, G. Wang, H. X. Xu, T. Cai, J. Liang, IEEE
Transactions on Antennas and Propagation **63**(11),
5144 (2015).

[25] F. Monticone, N. M. Estakhri, A. Alù, Physical
review letters **110**(20), 203903 (2013).

[26] A. O. Pinchuk, G. C. Schatz, J. Opt. Soc. Am. A
24(10), A39 (2007).

[27] O. Paul, B. Reinhard, B. Krolla, R. Beigang,
M. Rahm, Applied Physics Letters. 96(24),
241110 (2010).

[28] N. Yu, P. Genevet, M. A. Kats, F. Aieta,
J. P. Tetienne, F. Capasso, Z. Gaburro, Science
334(6054), 333 (2011).

[29] F. Aieta, P. Genevet, N. Yu, M. A. Kats, Z. Gaburro,
F. Capasso, Nano letters **12**(3), 1702 (2012).

[30] C. Li, D. Jian, H. Jun, D. Deng, H. Yu, L. Wang,
Y. Ma, Y. Hua, S. Xu, Ceram. Int. **42**(6),
6891 (2016).

[31] C. Li, H. Chen, Y. Hua, L. Yu, Q. Jiang, D. Deng,
S. Zhao, H. Ma, S. Xu, J. Lumin. **143**, 459 (2013).

[32] C. Li, J. Dai, H. Yu, D. Deng, H. Jun, L. Wang,
Y. Hu, S. Xu, RSC Adv. **6**(45), 38731 (2016).

[33] Cristian Della Giovampaola, Nader Engheta, Nature
Materials **13**(12), 1115 (2014).

[34] T. J. Cui, M. Q. Qi, X. Wan, J. Zhao, Q. Cheng,
Light: Sci. Appl. **3**(10), e218 (2014).

[35] X. G. Zhang, W. X. Jiang, H. L. Jiang et al., Nat.
Electron. **3**, 165 (2020).

[36] X. G. Zhang, Q. Yu, W. X. Jiang, Y. L. Sun, L. Bai,
Q. Wang, C. W. Qiu, T. J. Cui, Adv. Sci. **7**,
1903382 (2020).

[37] X. Bie, X. F. Jing, Z. Hong, C. X. Li, Appl. Opt.
57(30), 9070 (2018).

[38] G. Y. Lee, G. Yoon, S. Y. Lee, H. Yun, J. Cho,
K. Lee, H. Kim, J. Rho, B. Lee, Nanoscale **10**(9),
4237 (2018).

[39] K. Y. Liu, G. M. Wang, T. Cai, W. L. Guo,
Y. Q. Zhuang, G. Liu, Chinese Phys. B **27**(8),
084101 (2018).

[40] S. Liu, T. J. Cui, L. Zhang, Q. Xu, Q. Wang, X. Wan,
J. Q. Gu, W. X. Tang, M. Q. Qi, J. G. Han,
W. L. Zhang, X. Y. Zhou, Q. Cheng, Adv. Sci. **3**(10),
1600156 (2016).

[41] R. Y. Wu, C.B. Shi, S. Liu, W. Wu, T. J. Cui, Adv.
Opt. Mater. **6**(5), 1701236 (2018).

[42] S. Liu, T. J. Cui, Q. Xu, D. Bao, L. L. Du, X. Wang,
W. X. Tang, C. M. Ouyang, X. Y. Zhou, H. Yuan,
H. F. Ma, W. X. Jiang, J. G. Han, W. L. Zhang,
Q. Cheng, Light: Sci. Appl. **5**(5), e16076 (2016).

*Corresponding authors: fangbo@cjlu.edu.cn;
jingxufeng@cjlu.edu.cn